Available online at www.sciencedirect.com
SCIENCE DIRECT®
Journal of Nuclear Materials 343 (2005) 318–324
journal of nuclear materials
www.elsevier.com/locate/jnucmat

Microstructural control to improve the resistance to radiation embrittlement in vanadium

H. Kurishita [a,*], T. Kuwabara [a,1], M. Hasegawa [a], S. Kobayashi [b], K. Nakai [b]

[a] *International Research Center for Nuclear Materials Science, Institute for Materials Research, Tohoku University, Oarai, Ibaraki 311-1313, Japan*
[b] *Department of Materials Science and Engineering, Ehime University, 3 Bunkyo-cho, Matsuyama 790-8577, Japan*

Abstract

In order to improve the resistance to serious radiation embrittlement in refractory metals, a process for microstructural control is presented, with significance of controlling the substance, size, number density and distribution of dispersed particles. The process is applied to vanadium, a metal of group VA, with ultra-fine grains and finely dispersed, thermally stable particles. It is shown that the developed V–(1.6–2.6)%Y alloys have grain sizes between 170 and 340 nm and particle (Y_2O_3 and YN) sizes between 13 and 25 nm and exhibit the following noted features: (1) The microstructure is stable against vacuum heating at 1573 K for 1 h. (2) The vanadium matrix is very low in solute oxygen and nitrogen, which are responsible for environmental embrittlement of vanadium. (3) The alloys exhibit good tensile strength and elongation at low temperatures; approximately 1.5 times more strength and about 70% of the elongation compared with a V–4Cr–4Ti (Nifs-Heat-1) alloy. (4) The developed alloys show good resistance to neutron irradiation at 563 K to 0.25 dpa and 873 K to 0.60 dpa. These fabrication processes and noted features are applicable to other group VA metals such as tantalum.

1. Introduction

Refractory transition metals such as tungsten, group VIA, and tantalum, group VA, are candidate materials for spallation neutron source solid targets because of their superiority to other materials in many respects. However, tungsten exhibits serious embrittlement in several regimes; i.e., radiation embrittlement [1], low-temperature embrittlement, recrystallization embrittlement. Tantalum undergoes environmental embrittlement due to pick-up of gaseous interstitial impurities from the surroundings, and also suffers radiation embrittlement [2]. These types of embrittlement are microstructure sensitive and thus the key for achieving improvement in the resistance to embrittlement is to establish a process for microstructural control. Taking account of this respect, the authors have been making efforts to develop several refractory metals of group VIA and VA with improved resistance: molybdenum [3–8] and tungsten [7,9,10] and vanadium [11–15]. Vanadium is known to have quite similar physical and mechanical properties to tantalum, and the results on R&D for vanadium are applicable to tantalum. In this paper, the current status of the

* Corresponding author. Tel.: +81 29 267 4157; fax: +81 29 267 4947.
E-mail address: kurishi@imr.tohoku.ac.jp (H. Kurishita).
[1] Present address: Electronics & Materials R&D Laboratories, SUMITOMO ELECTRIC INDUSTRIES, LTD., Osaka Works, 1-1-3 Shimaya, Konohana-ku, Osaka 554-0024, Japan.

0022-3115/$ - see front matter © 2005 Elsevier B.V. All rights reserved.
doi:10.1016/j.jnucmat.2004.12.017

progress will be presented with focus on radiation embrittlement.

2. Microstructural control

The most effective microstructure to alleviate radiation embrittlement consists of fine grains and finely dispersed particles, the finer the better because grain boundaries and particles can serve as effective sinks for irradiation induced point defects. Such a microstructural refinement can be achieved by materials processing based on powder metallurgical (P/M) methods including mechanical alloying (MA) [16] and hot isostatic pressing (HIP). MA can provide powders with nano-sized grains of matrix material supersaturated with selected constituent elements and a very high density of dislocations. HIP leads to both the consolidation of MA treated powder and the formation of nano-sized dispersoids by precipitation.

During processing, it is quite important to control dispersed particles because the dispersoids (1) determine the final grain size and its distribution by pinning grain boundaries and inhibiting grain growth, (2) can have beneficial effects or detrimental effects on the ductility of their host material, and (3) are strongly affected by metal impurities introduced from grinding vessels and balls used for MA and gaseous impurities picked up during MA and HIP. It is essential to reduce such contamination, which is a critical issue for the processing procedure.

The control of dispersed particles involves the selection of the dispersion substance and the size, number density and distribution of the particles. The dispersion substances should be thermally stable and harmless to the ductility of the matrix. The particle size should be as small as possible for the following reasons; smaller particles tend to exhibit more coherency with the matrix, and the number density acceptable for preserving ductility increases for a certain volume fraction of the particles. For the particle distribution, homogeneous distribution is needed.

Control of the dispersion substance, size, number density and distribution of the particles is now considered.

Suppression of contaminant impurities from MA vessels and balls can be achieved by optimizing the MA condition. Such optimization will be made such as to meet three requirements: (1) to reach the final stage of MA, (2) to collect a sufficient amount of MA powder, and (3) to suppress processing contamination. For optimization of the milling parameters, the appropriate weight ratio of balls to powder, vessel rotation speed and milling time must be determined by trials. Suppression of gaseous impurities picked up during the fabrication process can be achieved by using a specially designed glove box, MA vessels and encapsulation of the MA powders in a metal can for HIPing. In the glove box, outgassing of the inside wall and all the necessities including the MA vessels and balls, spoons and balance is made at around 420 K and 10^{-6} Torr before introducing a purified Ar or H_2 gas (99.99999% purity). For the MA vessels, an oxygen-free copper gasket is used for sealing, which prevents exposure to the air when MA is conducted outside the glove box. No lubricants were added to the powders for MA. The MA treated powder was charged into a metal capsule in the glove box. Then the capsule with the MA powder was sealed by TIG welding during outgassing in a vacuum better than 1×10^{-6} Torr and then subjected to HIP. HIPing in a metal capsule permits consolidation of the MA treated powder without exposure to the air, at relatively low temperatures where grain growth is suppressed.

Provided the mixed powders of the starting materials are sufficiently mechanically alloyed, the size and density of the particles can be controlled by changing the conditions of HIP or VHP (vacuum hot pressing) and the subsequent annealing. Sintering by HIP or VHP with two-step heating at ~ 0.4 and $\sim 0.6T_m$ was found to be very effective to obtain a dispersion of nano-size particles, compared with one-step heating at $\sim 0.6T_m$ [17]. This is most likely due to enhanced nucleation relative to slow growth of the precipitates at $\sim 0.4T_m$ compared with the nucleation and growth of the particles in the one-step heating at $\sim 0.6T_m$ [17].

The distribution of the particles mainly depends on the MA processes. For instance, MA processes with the use of a planetary ball mill often resulted in a mixture of powders having different degrees of MA, leading to sintered compacts with heterogeneity in particle distribution and grain size distribution. To produce homogeneous MA treated powders, a 3MPDA (three mutually perpendicular directions agitation) ball mill was newly developed and used [10].

Therefore, in order to achieve a satisfactory level of microstructural control, each of MA and HIP processes should be carefully investigated.

3. Application of the method for microstructural control to vanadium

For vanadium, until recently there were no reports on successful microstructural control by P/M methods because vanadium is chemically very active and undergoes significant embrittlement due to contamination by atmospheric nitrogen and oxygen during P/M fabrication processes. However, it has been demonstrated that the application of the above glove box processing method to vanadium allows successful microstructural control without causing embrittlement [11–15]. It is a prerequisite to add yttrium into vanadium to make the

vanadium matrix free from solute oxygen and nitrogen by consuming all the oxygen and nitrogen impurities to form dispersoids of Y_2O_3 and YN [11]. In the following, the noted features of the developed vanadium alloys are shown in the unirradiated and irradiated states. Such features may be applicable to tantalum and niobium which belong to the same group VA as vanadium and are chemically active like vanadium, but have much higher melting points than vanadium.

Table 1 shows the chemical compositions, in wt%, of several V–Y alloys developed by MA and HIP from the starting materials of pure vanadium (particle size: <150 μm, 0.08 oxygen, 0.07 nitrogen) and pure yttrium (<750 μm, 1.56 oxygen, 0.05 nitrogen). Yttrium contents of 1.6–2.6% are high enough to consume all of the oxygen and nitrogen impurities contained in the materials. MA with 3PDA and two vessels and balls made of WC/Co was conducted, where the MA vessels with the powders and balls were cooled by a fan so that the vessel surface temperature was kept around 280 K. For TIG sealed mild steel capsules with the MA powders, about 35 mm in diameter and 53 mm in height, HIP was conducted at 1273 K for 3 h in an argon atmosphere and the compacts were then subjected to vacuum annealing as shown in Table 2. The contents of tungsten and cobalt arising from the milling vessels and balls during MA are 0.02–0.272 and <0.003–0.026 wt%, respectively.

Fig. 1 compares X-ray diffraction patterns taken from the mixed powder of the starting materials, MA treated powder and as-HIPed specimen of V–1.7Y, showing dissipation of the Y peaks for the MA powder. According to the equilibrium phase diagram of V–Y, the solubility of yttrium in vanadium is extremely small. However, Fig. 1 clearly shows that after MA the yttrium particles dissolve into the vanadium matrix and that Y_2O_3 and YN are formed by reaction of yttrium with solute oxygen and nitrogen during the HIP treatment.

A notable feature of the developed alloys in the unirradiated state is that the microstructure of the alloy is stable against high-temperature heating. Fig. 2 shows TEM bright field images of the grain structure and dispersed particles of V–1.7Y annealed at 1373 K for 1 h. The large, white areas in Fig. 2 probably correspond to pores formed during HIP. The average grain size and particle size and density for the V–Y alloys are shown in Table 2, together with the estimated volume fraction of Y_2O_3 and YN assuming that all of oxygen and nitrogen in Table 1 are consumed to form Y_2O_3 and YN. The volume fractions shown in Table 2 are considerably larger than those estimated from the data on particle size and density. This is probably due to large particles that were not observed by TEM. Annealing

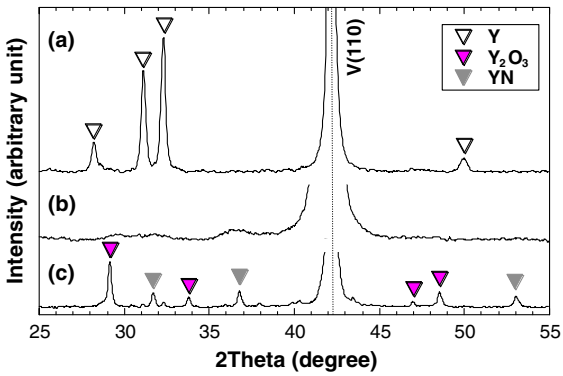

Fig. 1. X-ray diffraction patterns taken from (a) the mixed powder of the starting materials, (b) MA treated powder and (c) as-HIPed specimens of V–1.7Y.

Table 1
Chemical compositions of developed V–Y alloys (wt%)

Designation	O	N	C	Y	Co	W	Ar
V–1.6Y-1	0.171	0.078	0.0249	1.56	–	0.02	0.0014
V–1.6Y-2	0.141	0.075	0.0222	1.56	–	0.09	0.0012
V–1.7Y	0.181	0.104	0.0271	1.68	0.026	0.272	–
V–2.6Y	0.174	0.280	0.0166	2.57	<0.003	0.030	–

Table 2
The average grain size, size, density and volume fraction of the particles for developed V–Y alloys

Specimen	Annealing temperature (K)	Annealing period (h)	Average grain size (nm)	Average particle size (nm)	Total particle density ($10^{20}/m^3$)	Volume fraction (%)
V–1.6Y-1	1273	1	290	22	1.7	1.5
V–1.6Y-2	1273	1	303	25	1.8	1.4
V–1.7Y	1373	1	339	13	–	1.7
V–2.6Y	1273	1	170	21	3.6	2.9

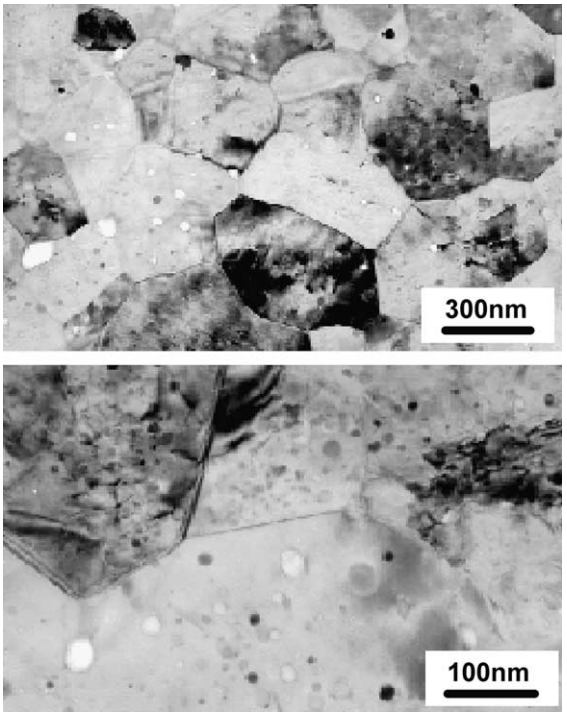

Fig. 2. TEM micrographs showing the grain structure and dispersed particles in V–1.7Y annealed at 1373 K for 1 h.

experiments up to 1573 K for 1 h in V–1.7Y revealed that the average grain size and particle size for V–1.7Y still remained as small as 750 nm and 23 nm, respectively. An annealing temperature of 1573 K corresponds to the high homologous temperature of $0.72T_m$ [15].

Another feature is that the vanadium matrix in the alloys is free from solute oxygen and nitrogen. Since solution hardening by oxygen and nitrogen is reported as a function of oxygen and nitrogen concentrations and is very large [18], approximate contents of oxygen and nitrogen in the matrix can be estimated from the measured hardness of the matrix free from grain boundaries and dispersoids. However, it is quite difficult to obtain the proper hardness value of the fine-grained matrix phase with dispersed particles of the developed vanadium alloys. Therefore the following method was used.

A HIPed compact with coarse-grained and fine-grained regions was carefully prepared by blending slightly MA treated powders into fully MA treated powders of V–1.6Y. The coarse-grained regions derived from the slightly MA treated powders and occupied about 25–30% of the compact were confirmed to have grain sizes large enough to measure the Vickers microhardness of the grain interior and contain very few dispersoids because of the absence of yttrium supersaturated in the matrix by MA. The contents of solute nitrogen and oxygen in the coarse-grained regions are considered to be very low and close to those in fine-grained regions because during HIPing at 1273 K for 3 h solute nitrogen and oxygen can diffuse over long distance to meet supersaturated yttrium exiting in the surrounding fine-grained regions. It can be hence concluded that the hardness measured in the coarse-grained regions is very close to that of the matrix free from grain boundaries and dispersoids in the fine-grained regions. The result on hardness measurements for the coarse-grained regions, together with an indentation on the specimen surface, is shown in Fig. 3. Here the Vickers microhardness of EB melted vanadium was measured by the same apparatus at the same very low load (10gf) as that of V–1.6Y–2. The hardness of the vanadium matrix is 56HV and is lower than that of a

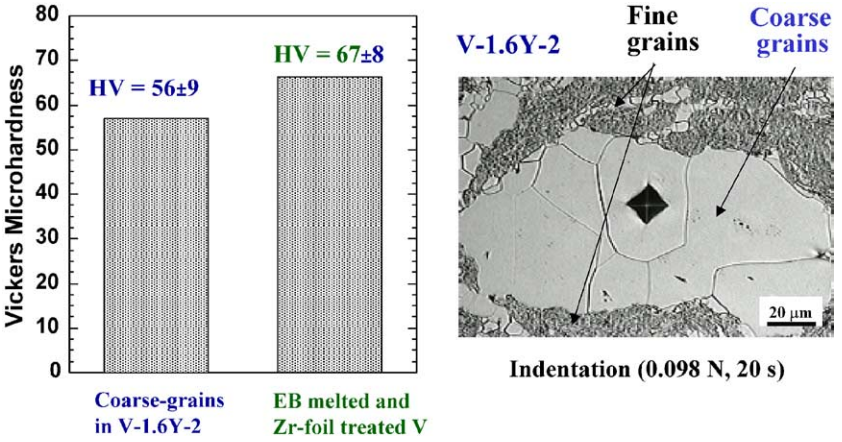

Fig. 3. Comparison of Vickers microhardness for coarse-grains in V–1.6Y-2 and for EB-melted and Zr-foil treated vanadium containing 24 wppm oxygen and 2 wppm nitrogen, indicating that the vanadium matrix in V–1.6Y-2 is very low in solute oxygen and nitrogen.

very high pure vanadium specimen containing only 24 wppm oxygen and 2 wppm nitrogen [19], which was prepared by electron beam melting and purification by the Zr-foil method. This indicates that the vanadium matrix in the alloys has lower solute oxygen and nitrogen contents than the pure vanadium specimen.

As a result of the purification of the matrix, the developed alloys are expected to exhibit good tensile ductility. Fig. 4 shows stress–strain curves for V–1.7Y tested at a high strain rate of $10\ s^{-1}$ and at low temperatures, in comparison with those for V–4Cr–4Ti, which was prepared by electron beam melting and is reported to have excellent ductility and toughness [20,21]. Here, both the V–1.7Y and V–4Cr–4Ti specimens were machined into the identical dimensions and tested by a servo-hydraulic fatigue testing machine (Shimadzu Servopulser of 50-kN capacity equipped with a 5-kN shear-type load cell). High strain-rate tests are known to be more effective in elucidating difference in ductility between materials or material conditions than low strain-rate tests. V–1.7Y shows almost 1.5 times the strength and about 70% of the elongation compared with V–4Cr–4Ti, resulting in almost the same toughness as V–4Cr–4Ti.

Another noted feature is that the developed alloys exhibit good resistance to radiation hardening which is responsible for radiation embrittlement. Table 3 shows the specimens and conditions for neutron irradiation performed in JMTR (Japan Materials Testing Reactor). After irradiation the specimens were subjected to PIE (post irradiation examination) such as hardness measurements and microstructural examinations. The irradiation temperature of 563 K is known to be low enough to cause serious radiation embrittlement in V–4Cr–4Ti and regular vanadium.

Fig. 5 shows Vickers microhardness before and after irradiation. It should be noted that the increase in HV due to irradiation, i.e., radiation hardening, is very small even for irradiation at 563 K, although 1073 K-irradiation causes appreciable hardening, which will be mentioned later.

Fig. 6 shows TEM microstructures of V–1.6Y-1 irradiated at 563 K; (a) a bright field image and (b) a dark field image by (420)Y_2O_3. In Fig. 6(a) Y_2O_3 particles and large voids of 10–50 nm in diameter are marked by horizontal and vertical arrows, respectively. The large voids exist near grain boundaries and Y_2O_3 particles. It is known that grain boundaries and dispersed particles are effective sinks for irradiation induced defects and voids are distributed apart from such sinks. In view of the aspect that the pores mentioned in Fig. 2 are preferentially formed near grain boundaries and dispersoids, it is more likely that such pores act as nucleation sites for large voids.

In addition to such large voids, a high density of small voids of 2–3 nm in diameter were observed for the same specimens, as shown in Fig. 7, which corresponds to an enlarged micrograph of the central region

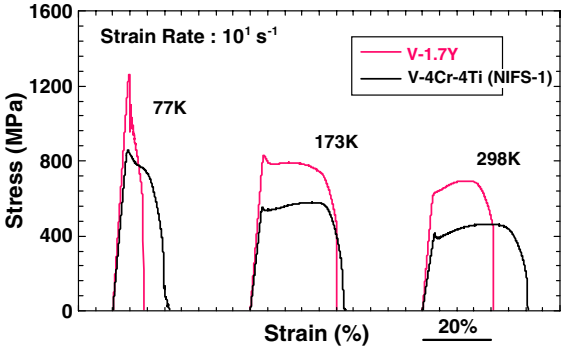

Fig. 4. Comparison of low-temperature dynamic tensile properties for V–1.7Y and V–4Cr–4Ti.

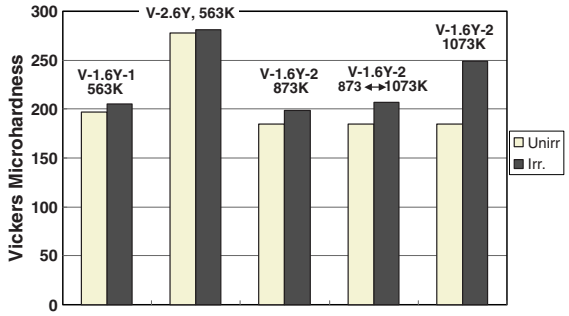

Fig. 5. Vickers microhardness before and after neutron irradiation in various conditions for V–1.6Y and V–2.6Y.

Table 3
Neutron irradiation condition in JMTR and specimens used

Specimen	Irradiation temperature (K)	Fast neutron flux (>1 MeV, $\times 10^{17}$ n/m^2 s)	Period (h)	DPA	Atmosphere
V–1.6Y-1	563	3.1	1175	0.25	He
V–2.6Y	563	3.1	1175	0.25	He
V–1.6Y-2	873	15.6	570	0.60	He
V–1.6Y-2	873 $\Longleftrightarrow$ 1073/6 cycles*	10.7	570	0.40	He
V-1.6Y-2	1073	18.5	570	0.70	He

* Temperature cycle irradiation between 873 and 1073 K with 6 cycles [22].

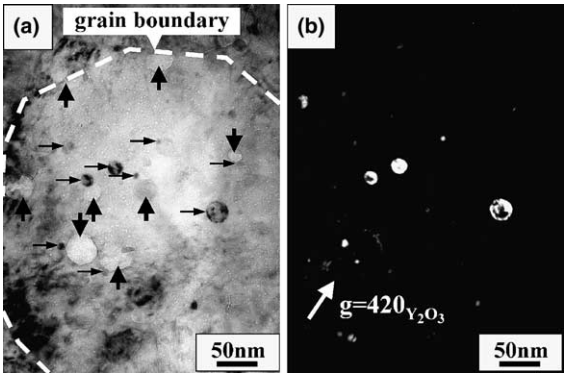

Fig. 6. TEM micrographs for V–1.6Y-1 irradiated at 563 K to 0.25 dpa: (a) bright field image and (b) dark field image by $(420)_{Y_2O_3}$. Y_2O_3 particles and large voids are indicated by horizontal and vertical arrows in (a) [12].

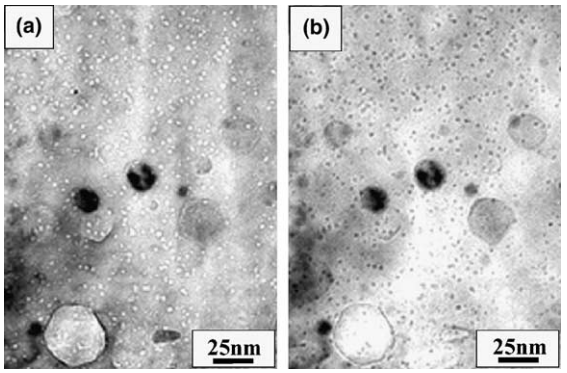

Fig. 7. TEM micrographs showing the distributions of voids for V–1.6Y-1 irradiated at 563 K to 0.25 dpa; (a) under-focus and (b) over-focus [12].

in Fig. 6. The density of small voids was estimated to be $1.8 \times 10^{23}/m^3$. The very small radiation hardening measured in this specimen, Fig. 5, shows that these voids are not effective obstacles to dislocation motion at room temperature. This suggests that at room temperature moving dislocations can overcome such short range obstacles by thermally activated processes. Such short range obstacles, however, will become effective obstacles to dislocation motion and cause radiation hardening as the test temperature decreases below room temperature where the contribution of thermal activation to flow stress becomes less significant.

Fig. 8 presents a TEM microstructure of V–2.6Y irradiated at 563 K, which clearly shows that there are few or no small voids. However, this remarkable difference in the occurrence of small voids between V–1.6Y-1 (many voids) and V–2.6Y (no voids) is not clearly

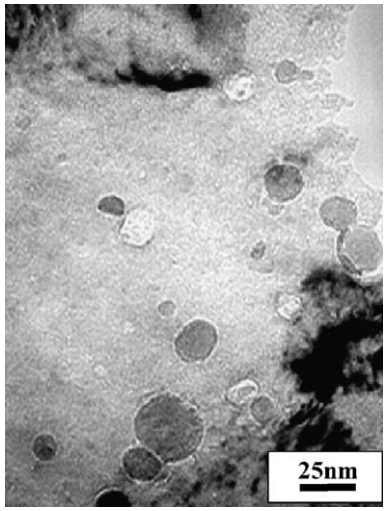

Fig. 8. TEM micrograph showing absence of small voids for V–2.6Y irradiated at 563 K to 0.25 dpa [12].

explained yet, but a possible explanation is: the density of sinks such as grain boundaries and dispersoids is considerably higher in V–2.6Y than in V–1.6Y-1 (see Table 2).

Assuming that all of the oxygen and nitrogen shown in Table 1 is consumed to form Y_2O_3 and YN during HIP or subsequent annealing before irradiation, the amounts of the residual, uncombined yttrium (solute or fine dispersoids) are estimated to be 0.63 wt% for V–1.6Y-2. The uncombined yttrium may lead to additional formation of Y_2O_3 and YN particles providing that solute oxygen and nitrogen are available. Fig. 9 shows a particle size distribution before and after irradiation at 1073 K for V–1.6Y-2. It is obvious that the particle density and large-sized particles increase after irradiation, with the total density from $1.78 \times 10^{20}\ m^{-3}$ before irradiation to $2.24 \times 10^{20}\ m^{-3}$ after irradiation,

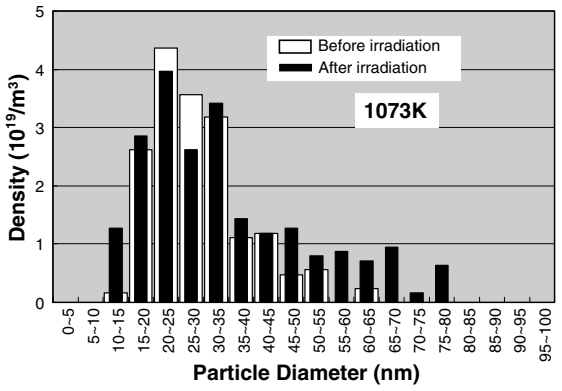

Fig. 9. Particle size distributions before and after irradiation at 1073 K for V–1.6Y-2 [12].

resulting in approximately doubled particle volume fraction after irradiation. For the other irradiation conditions no increase in volume fraction of particles were observed [12]. Therefore, it is reasonable to say that the increased density of Y_2O_3 and YN particles is due to reaction of residual, uncombined yttrium with oxygen and nitrogen picked up from the surroundings during the 1073 K irradiation and that unreacted, excess oxygen and nitrogen in solution caused the hardening observed after the 1073 K irradiation.

4. Conclusions

A method for microstructural control to alleviate radiation embrittlement in refractory metals was presented. The application of the method to vanadium, group V, allowed to introduce fine grains and finely dispersed, thermally stable particles of Y_2O_3 and YN in the microstructure without losing most of its good ductility before irradiation. It was found that the developed V–(1.6–2.6)Y alloys show the following noted features:

(1) The microstructure is stable against vacuum heating at 1573 K for 1 h.
(2) The vanadium matrix is deduced to be free from solute oxygen and nitrogen, which are responsible for embrittlement.
(3) The alloys exhibit a good tensile strength and elongation even below room temperature at a strain rate of 10 s^{-1}; approximately 1.5 times the strength and about 70% of the elongation compared with a V–4Cr–4Ti (Nift-Heat-1) alloy.
(4) The developed alloys show good resistance to neutron irradiation hardening at 563 and 873 K to 0.25 and 0.60 dpa, respectively.

Acknowledgement

The authors would like to express their gratitude to Drs Y. Aono and H. Arakawa, Hitachi Research laboratory, Hitachi, Ltd., for their help with use of HIP apparatus and to Dr S. Matsuo for his review of the paper.

References

[1] For instance I. Smid, M. Akiba, G. Vieider, L. Plöchl, J. Nucl. Mater. 253–263 (1998) 160.
[2] For instance H. Ullmaier, F. Carsughi, Nucl. Instrum. and Meth. B 101 (1995) 406.
[3] H. Kurishita, Y. Kitsunai, Y. Hiraoka, T. Shibayama, H. Kayano, Mater. Trans. JIM 37 (1996) 89.
[4] H. Kurishita, Y. Kitsunai, T. Shibayama, H. Kayano, Y. Hiraoka, J. Nucl. Mater. 233–237 (1996) 557.
[5] Y. Kitsunai, H. Kurishita, M. Narui, H. Kayano, Y. Hiraoka, J. Nucl. Mater. 239 (1996) 253.
[6] H. Kurishita, Y. Kitsunai, H. Kayano, Y. Hiraoka, T. Takida, T. Igarashi, in: G. Kneringer, P. Rodhammer, P. Wilhartitz (Eds.), Proceedings of the 14th International Plansee Seminar, vol. 1, 1997, p. 287.
[7] H. Kurishita, Y. Kitsunai, T. Kuwabara, M. Hasegawa, Y. Hiraoka, T. Takida, T. Igarashi, J. Plasma Fus. Res 75 (1999) 594 (in Japanese).
[8] H. Kurishita, Basic studies in the field of high-temperature engineering, OECD (2002) 103.
[9] Y. Kitsunai, H. Kurishita, M. Narui, H. Kayano, Y. Hiraoka, T. Igarashi, T. Takida, J. Nucl. Mater. 271&272 (1999) 423.
[10] Y. Ishijima, H. Kurishita, K. Yubuta, H. Arakawa, M. Hasegawa, Y. Hiraoka, T. Takida, K. Takebe, J. Nucl. Mater. 329–333 (2004) 775.
[11] T. Kuwabara, H. Kurishita, M. Hasegawa, J. Nucl. Mater. 283–287 (2000) 611.
[12] S. Kobayashi, Y. Tsuruoka, K. Nakai, H. Kurishita, Mater. Trans. 45 (2004) 29.
[13] S. Kobayashi, Y. Tsuruoka, K. Nakai, H. Kurishita:, J. Nucl. Mater. 329–333 (2004) 447.
[14] S. Oda, H. Kurishita, Y. Tsuruoka, S. Kobayashi, K. Nakai, H. Matsui, J. Nucl. Mater. 329–333 (2004) 462.
[15] T. Kuwabara, H. Kurishita, M. Hasegawa, Mater. Sci. Eng., submitted for publication.
[16] J.S. Benjamin, Met. Trans. 1 (1970) 2943.
[17] Y. Ishijima, H. Kurishita, K. Yubuta, H. Arakawa, M. Hasegawa, Y. Hiraoka, T. Takida, K. Takebe, in preparation.
[18] R.C. Svedberg, R.W. Buckman, Int. Met. Rev. 25 (1980) 223.
[19] K. Fukumoto, H. Matsui, private communication.
[20] T. Muroga, T. Nagasaka, A. Iiyoshi, A. Kawabata, S. Sakurai, M. Sakata, J. Nucl. Mater. 283–287 (2000) 711.
[21] T. Nagasaka, T. Muroga, M. Imamura, S. Tomiyama, M. Sakata, Fus. Technol. 39 (2001) 659.
[22] M. Narui, H. Kurishita, H. Kayano, T. Sagawa, N. Yoshida, M. Kiritani, J. Nucl. Mater. 212–215 (1994) 1665.